Full Length Article

On the transcritical mixing of fuels at diesel engine conditions

Cyril Crua [a,*], Julien Manin [b], Lyle M. Pickett [b]

[a] Advanced Engineering Centre, University of Brighton, Brighton BN2 4GJ, United Kingdom
[b] Sandia National Laboratories, 7011 East Avenue, 94550 Livermore, CA, United States

HIGHLIGHTS

- We observed microscopic fuel droplets transitioning to supercritical fluid.
- A conceptual model and criteria for the transition to diffusive mixing are proposed.
- Surface tension and primary atomization remain important features of diesel mixing.
- Transition to diffusive mixing regime is driven by gas pressure and temperature.
- Timescales and fluid morphology for diffusive mixing are driven by fuel properties.

GRAPHICAL ABSTRACT
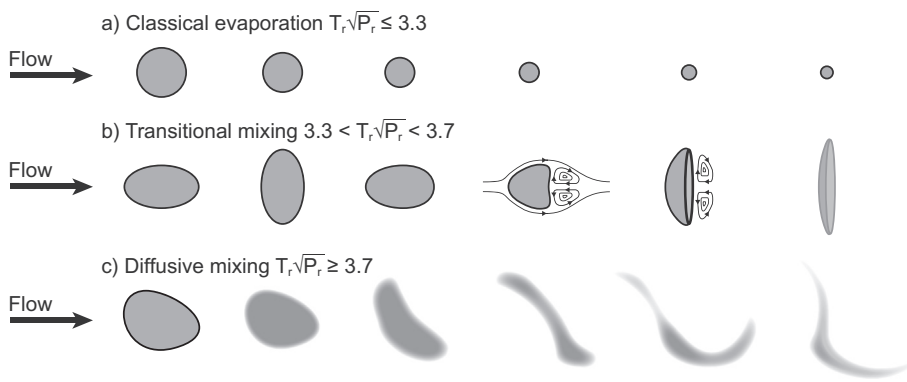
ARTICLE INFO

ABSTRACT

Whilst the physics of both classical evaporation and supercritical fluid mixing are reasonably well characterized and understood in isolation, little is known about the transition from one to the other in the context of liquid fuel systems. The lack of experimental data for microscopic droplets at realistic operating conditions impedes the development of phenomenological and numerical models. To address this issue we performed systematic measurements using high-speed long-distance microscopy, for three single-component fuels (n-heptane, n-dodecane, n-hexadecane), into gas at elevated temperatures (700–1200 K) and pressures (2–11 MPa). We describe these high-speed visualizations and the time evolution of the transition from liquid droplet to fuel vapour at the microscopic level. The measurements show that the classical atomization and vaporisation processes do shift to one where surface tension forces diminish with increasing pressure and temperature, but the transition to diffusive mixing does not occur instantaneously when the fuel enters the chamber. Rather, subcritical liquid structures exhibit surface tension in the near-nozzle region and then, after time surrounded by the hot ambient gas and fuel vapour, undergo a transition to a dense miscible fluid. Although there was clear evidence of surface tension and primary atomization for n-dodecane and n-hexadecane for a period of time at all the above conditions, n-heptane appeared to produce a supercritical fluid from the nozzle outlet when injected at the most elevated conditions (1200 K, 10 MPa). This demonstrates that the time taken by a droplet to transition to diffusive mixing depends on the pressure and temperature of the gas surrounding the droplet as well as the fuel properties. We summarise our observations into a phenomenological model which describes the morphological evolution and transition of microscopic droplets from *classical evaporation* through a *transitional mixing* regime

* Corresponding author.
  E-mail address: c.crua@brighton.ac.uk (C. Crua).
  URL: http://www.brighton.ac.uk/staff/crua (C. Crua).

and towards *diffusive mixing*, as a function of operating conditions. We provide criteria for these regime transitions as reduced pressure–temperature correlations, revealing the conditions where transcritical mixing is important to diesel fuel spray mixing.

1. Introduction

The diesel fuel injection process may be described as transcritical under most operating conditions: the temperature of the fuel inside the injector is well below the critical temperature, while the pressure and temperature of the in-cylinder gas both exceed the fuel's critical values. Whilst there is potential for the liquid to transition into a supercritical fluid when exposed to elevated pressures and temperatures, the fuel does not mix with the ambient gas as in a single-component system and therefore the state of the fluid will depend on the local heat and mass transfer, including the interdiffusion of the various species involved. Hence a transition from a two-phase mixing regime, with classical evaporation and surface tension forces, to a single-phase regime dominated by diffusion and convection without surface tension forces may be hypothesised [1], but the mechanism of this transition is yet to be defined. In particular, one cannot rely upon a knowledge of the critical properties of the gas or liquid, since a fuel injection system mixing with gas is multi-component. In addition, calculation of critical properties for given mixtures of fuel and gas at equilibrium is not necessarily relevant since, initially, the components are completely separated, and as they mix together, may never reach given mixture states [2]. Consequently, uncontroversial evidence of the mechanism of transcritical mixing is still needed for operating conditions and spatial scales representative of combustion engines.

The lack of fundamental understanding of transcritical fuel injection is due to the considerable challenges involved in generating, and characterizing, microscopic droplets in a thermodynamically-controlled environment representative of internal combustion engines. Researchers have attempted to develop experiments with well-controlled boundary conditions to leverage our understanding of the physics of transcritical mixing. Suspended droplet experiments are commonly used to characterise the evaporation of liquids, but they cannot be extended to supercritical fluid states as the approach requires surface tension to attach a droplet onto a fibre or capillary tube [3]. Droplet stream generators also fail to function reliably at elevated temperatures as the reduced surface tension inhibits the development of Rayleigh instabilities, which is the main mechanism used to create the droplet stream. To circumvent these issues, Weckenmann and coworkers generated droplets near supercritical conditions using a 200 μm steel capillary tube and forced the detachment of droplets by applying an electric field [4]. The acetone droplets they generated were 2 mm in diameter and, although it should be possible to generate smaller droplets using this approach, the internal diameter of the capillary tube imposes a lower limit on droplet diameters that is much larger than droplet sizes typically found in internal-combustion engines. One should also note that drop-on-demand and capillary jets are known to result in long-lasting residual motion inside the liquid droplet they generate [5], which will affect the internal mass transfer in a way that is not representative of a conventional spray system. The difficulties associated with the production of fuel droplets into a supercritical environment can be overcome by using a fuel injector to generate a distribution of droplets in a high pressure and temperature vessel. However, optically resolving individual droplets becomes particularly challenging and researchers using this approach have focused on attempting to identify macroscopic changes in the physical appearance of the spray plumes as indirect evidence of a change in mixing process [6–8]. Whilst a 'supercritical injection' would produce a jet with an optically diffused boundary, it is also known that several optical effects result in a loss of sharpness of a two-phase spray boundary. Artificially blurred liquid/gas interfaces could occur due to: motion-induced blurring of high-speed droplets; the presence of a 'shroud' of dense fuel vapour around liquid droplets; beam steering through significant fluctuations in density gradients within the ambient gas [9]. The shroud of vapour surrounding liquid also changes with operating conditions, even under classical droplet evaporation pathways. With increasing far-field (ambient) gas temperatures, vaporisation is accelerated, and with increasing ambient gas pressure, mixing of these high-temperature gases into the fuel spray is accelerated [10]. Thus, there is a need to consider changes in the spatial location and time history of classical evaporation processes as pressure and temperature are varied. To mitigate these uncertainties Chehroudi compared the visual appearance of sprays with their growth rate [11], suggesting that they behaved as incompressible variable-density gas jets when at conditions above the critical point of the injectant, and proposed a phenomenological model for jet growth rate as a function of the gas/liquid density ratio [12]. More recently, evidence that the time history of the mixture is important has come from recent work by Dahms and coworkers [13]. Progressing beyond an analysis of the vapour-liquid interface at equilibrium, a non-equilibrium analysis shows that surface tension does not vanish instantly [14]. Rather, the authors found that the interface thickens in time beyond the equilibrium solution, favouring the reduction in intermolecular forces, i.e., surface tension.

These macroscopic-scale experiments and theoretical models demonstrate that direct evidence of individual droplets transitioning from liquid phase to supercritical fluid has been sorely missing. Improving our understanding of fuel atomization and mixing processes at the microscopic scale is essential for the development of physically-correct models and the validation of numerical simulations [15,13,14,2]. Hence a conceptual model of the transition process at the microscopic scale and at engine-relevant conditions has been incomplete. In this paper we address some of these limitations, by combining recent advances in high-resolution microscopy at the University of Brighton [16–20] and high-speed microscopy at Sandia National Laboratories [9], to put the phenomenological description of transcritical fuel mixing on a firmer basis:

- We describe high-speed high-resolution microscopic visualizations of droplets transitioning from two-phase evaporation to single-phase diffusive mixing at engine-relevant conditions.
- We show clear evidence of surface tension and primary atomization at all these conditions for *n*-dodecane and *n*-hexadecane (Section 3.1). We also observed clear evidence of surface tension for *n*-heptane, except under the most elevated conditions (1200 K, 10 MPa) where diffusive mixing appeared to take place within 500 μm of the nozzle exit (Section 3.3).
- The time taken by a droplet to transition to diffusive mixing depends on the local gas pressure and gas temperature (Section 3.2), as well as on the fuel's physical properties (Section 3.3).
- We summarise our observations into a phenomenological model which describes the morphological evolution of microscopic droplets before, during, and after their transition from

evaporation to diffusive mixing (Section 3.4). We provide criteria for these transitions as pressure–temperature charts for each fuel tested, revealing the conditions where transcritical mixing is relevant to diesel fuel sprays.

2. Experimental setup and data acquisition

2.1. Pressure vessel and spray system

Experiments were conducted using a preburn combustion vessel [21]. This constant-volume chamber is of cubical shape, offering six faces that can be fitted with transparent sapphire windows or metal ports. The thermodynamic conditions simulated inside the chamber cover a wide range of temperatures (up to 1400 K) and pressures (35 MPa) and are achieved after combustion of a preburn mixture of combustible gases composed of C_2H_2, H_2, N_2 and O_2. After the spark-ignited preburn combustion is complete, the internal temperature and pressure conditions decrease due to heat transfer to the vessel walls during a cool-down period of several seconds. The fuel is injected when the desired ambient conditions are reached during the cool-down. During this campaign, the line-of-sight arrangement of the optical experiments required two opposite faces to be equipped with optical windows on both sides of the spray (Fig. 1). The spray is back-illuminated through one sapphire window and imaged through another sapphire window on the other side. Note that the pair of spark plugs used to ignite the preburn mixture are located at the top of the chamber and are not shown in this schematic.

Sprays of normal alkanes (*n*-heptane, *n*-dodecane, *n*-hexadecane) were injected by a commercial common-rail solenoid-actuated injector equipped with a single-hole nozzle. The axial orifice located at the tip of the nozzle has a diameter of 0.180 mm and features a converging conical shape (KS 1.5). We selected a single-hole axially-drilled nozzle to ensure that the fuel spray would develop along the centre of the combustion vessel, where the thermodynamic conditions are best controlled. The fuel injector was temperature-controlled to ensure that the state of the fuel prior to injection was both known and consistent across the different operating conditions, with a target temperature of 90 °C [21]. The nozzle's temperature was measured using a dummy injector fitted with a thermocouple to adjust the injector cooling system for repeatable measurements, as described by Meijer et al. [22]. The rest of the injection system is composed of a production-type common-rail, high-pressure lines and an air-driven high-pressure fuel pump. The injection pressure during these experiments was varied between 50 and 150 MPa, but the lower injection pressure condition was preferred because of the broader droplet size distribution.

2.2. Boundary conditions

The ambient conditions tested in this work ranged from pressures below 2 MPa to above 10 MPa and temperatures around 700 to 1200 K, with corresponding gas densities from 6 to 38 kg m^{-3}. Hence most of the ambient gas conditions were above the nominal critical points of the single-component fuels (Table 1). The gas temperatures reported in this work were based on direct calibration through thin-wire thermocouple measurements downstream of the injector tip as will be described below. As mentioned above, a premixed combustible gas mixture is ignited to reach the desired thermodynamic conditions (temperature and pressure), the sprays are therefore injected into the products left-over by the premixed combustion process, with the following volume fractions:

Nitrogen	N_2	89.71%
Carbon dioxide	CO_2	6.52%
Water	H_2O	3.77%

The pressure inside the vessel was recorded as a function of time during the premixed combustion, cool-down and fuel injection event, using high-accuracy piezo-resistive pressure sensors. Obtaining information about local temperature is more challenging due to the short timescales involved. As demonstrated by Meijer et al. [22], the temperature distribution is location dependent, with a slight reduction when approaching one of the chamber walls, especially the wall near the injector because of the temperature control (cooling). Thin-wire thermocouple measurements were performed to measure the temperature of the environment in the
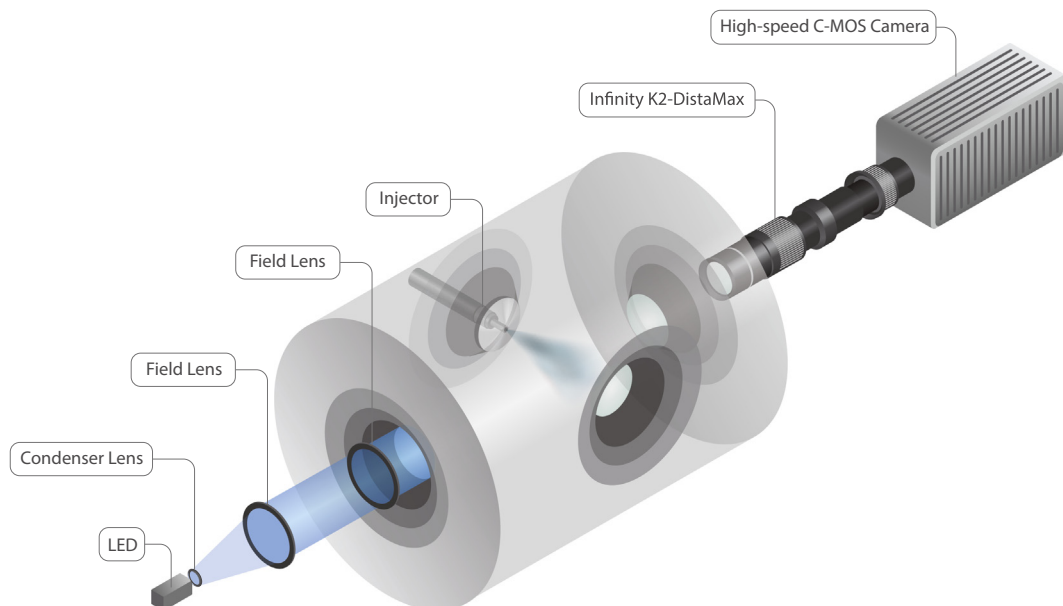

Fig. 1. Schematic of the combustion vessel showing the optical accesses and the long-distance microscope imaging system. The high-speed camera and microscope were mounted on a 3-axis traverse. A blue light-emitting diode (LED) was used to provide the back illumination.

Table 1
Ranges of reduced temperatures and pressures for the fuels used in this study. Both P_r and T_r are calculated by dividing the ambient gas (P_g, T_g) values by the critical values of the fuel (P_c, T_c).

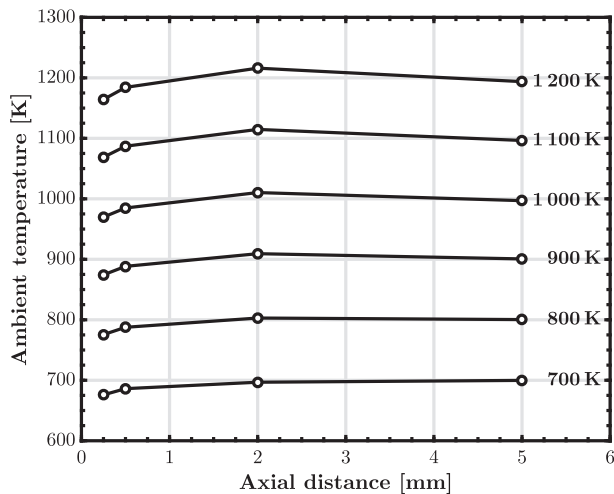|	n-Heptane C_7H_{16}	n-Dodecane $C_{12}H_{26}$	n-Hexadecane $C_{16}H_{34}$
Liquid density at (6 MPa, 363 K)	631 kg m^{-3}	704 kg m^{-3}	727 kg m^{-3}
Critical point temperature (T_c)	540 K	658 K	722 K
Critical point pressure (P_c)	2.7 MPa	1.8 MPa	1.4 MPa
Reduced temperature range ($T_r = T_g/T_c$)	[1.3, 2.2]	[1.1, 1.8]	[1.0, 1.7]
Reduced pressure range ($P_r = P_g/P_c$)	[0.7, 3.9]	[1.1, 5.8]	[1.4, 7.6]
Density ratio range ($\rho_r = \rho_g/\rho_l$)	[0.010, 0.060]	[0.009, 0.050]	[0.008, 0.050]

Fig. 2. Temperature measurement via thin-wire thermocouple experiments showing the local temperature distribution for the range of targeted ambient temperatures as a function of axial distance from the injector orifice exit.

■ n-heptane ● n-dodecane ▲ n-hexadecane

Fig. 3. Pressure–temperature diagram showing the targeted experimental conditions. The black symbols indicate the critical points for the three pure alkanes used in this study. The red symbol indicates the ECN 'Spray A' standard test point.

near-nozzle region for the different operating conditions tested. The description and procedures provided by Meijer et al. [22] about the thin-wire thermocouple experiments in the constant-volume pressure vessels of the Engine Combustion Network apply to the present temperature measurements.

In this study we used our high-resolution imaging system to accurately position the thermocouple junction at 0.25, 0.50, 2.0 and 5.0 mm from the injector tip along the spray axis. Consistent with previous measurements [22], the ambient gas temperature prior to injection was uniform in the horizontal plane of the vessel downstream of approximately 1 mm (Fig. 2). The most significant temperature deviation was observed within the cooler thermal boundary layer near the injector, but the deviation did not make the ambient boundary condition undefined. At a distance of 0.25 mm from the injector tip, the gas temperatures were only 2–3.5% cooler than the uniform core gases downstream of 1 mm. In addition, observations of liquid structure characteristics were made downstream of the thermal boundary layer (1 mm) where the ambient gases are more uniform in temperature. Hence, mixing between liquid fuel exiting the injector and the hot ambient gases occurs within well-defined boundary conditions.

The targeted operating conditions are presented on a pressure–temperature plot in Fig. 3. The data covered a wide range of reduced pressures (P_r) and temperatures (T_r), which are listed in Table 1. Both P_r and T_r are calculated by dividing the ambient gas (P_g, T_g) values by the critical values of the fuel (P_c, T_c). We acknowledge that constructing P_r and T_r using multi-component combinations of ambient and fuel properties has no thermodynamic analogue, but is performed as a simple way to summarise the data range. This study accesses conditions at $T_r > 1$ to encourage understanding at transcritical conditions.
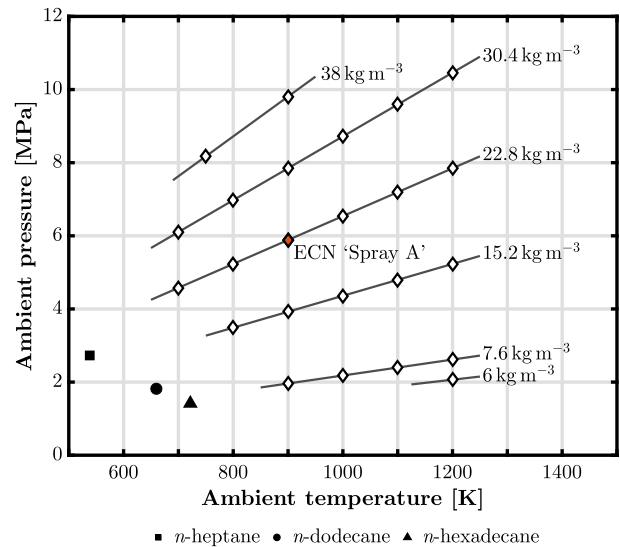
2.3. Optical system, spatial resolution and defocus

The optical system developed to acquire detailed high-speed videos of high-pressure sprays was composed of a long-working-distance microscope lens, a high-speed CMOS camera (Photron SA-X2) and a custom-built illumination system. The illumination in this line-of-sight configuration relied on diffused lighting to avoid non-uniform illumination intensities and reduce the effects of beam-steering [9]. The LED system designed for this application produced pulses of light at 450 nm (20 nm FWHM) for 200 ns at high repetition rates, for instantaneous peak power in excess of 15 W. A condenser lens and two Fresnel lenses collected the light rays from the LED to concentrate them onto an area slightly larger than the camera's field of view. The high-speed CMOS camera was equipped with the long-distance microscope lens configured for a magnification of 8×, for most of the experiments. Based on the magnification and the camera sensor pixel size, the final optical scale is 2.5 μm/pixel. The vast majority of the experiments were performed with a 1024 pixel long region of interest and frame rates ranging from 10,000 to 18,000 frames per second (fps). Although the camera exposure time was set to 2 μs, the illumination system pulse duration determined the exposure timescale ($\approx$ 200 ns). The numerical aperture of the system for the main configuration was 0.16, corresponding to a collection angle of about 320 mrad. The diffraction limit for our optical system was less than 2 μm, or less than a pixel, and as such did not limit its performance. Additional experiments were performed to visualise a larger field of view ($\approx$ 11 mm); in that configuration the long-distance microscope

objective was set to produce a digital image resolution greater than 11 μm/pixel.

Several parameters are available in the literature to evaluate the optical resolution of an imaging system. The Abbe or Rayleigh criteria provide theoretical limits of the imaging system's resolution, but these parameters do not consider lens imperfections and other optical distortions caused by fluctuations in refractive index gradients, and system vibrations, for instance. In order to characterise the response of our optical system, and more specifically its resolution, we measured its Modulation Transfer Function (MTF) [23]. The MTF was evaluated using the slanted edge method, which is based on the intensity slope recorded by the system as a response to a sharp inclined edge [24]. A knife-edge was mounted in the vessel, such that it was coincident with the axis of the spray, to probe the optical quality of the system as close as possible to the actual measurement region. Although the optical scale of the system is 2.5 μm/pixel, its effective resolution at 10% contrast was found to be closer to 2.8 μm (Fig. 4).
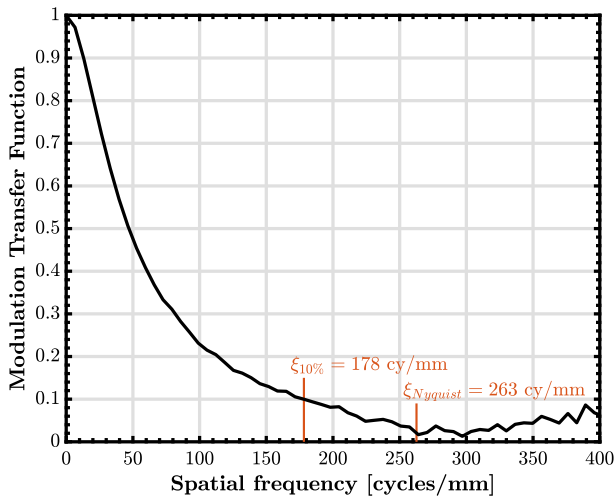

Fig. 4. Modulation transfer function (MTF) for the optical system with 8× magnification, measured using the slanted edge technique [24]. Although the scale factor for the optical system is 2.5 μm/pixel, its effective optical resolution at 10% contrast is closer to 2.8 μm ($\xi_{10\%}$ = 178 cy/mm).

For optical experiments performed in highly pressurised gaseous environment, the sharpness of the images is of primary interest as degradation of focus would affect the ability to detect spray features such as small droplets. This degradation in image sharpness can occur due to fluctuations in density gradients within the ambient gas, initiated by the chamber's preburn, which result in localised arbitrary shifts of the imaging system's focal position. Additional refractive index gradients also occur as a result of the evaporation of the spray, which results in local density fluctuations [9]. The response of an imaging system to changes in density or refractive index is not trivial in randomly oriented refractive index gradients such as those found within the pressure vessel. Hence one cannot expect the nominal resolution and depth of field of the imaging system to be representative of those during actual operating conditions, thus making it essential to characterise these parameters in situ.

As in many microscopy applications, characterizing the effective depth of field of the optical system is of particular interest. This is normally straightforward but significant complications are introduced when microscopy is applied to high pressure and temperature environments [18]. The characterization of the effective depth of field becomes particularly important, and challenging, when applying microscopy in a combustion vessel such as the one used in our study, where intense and transient density gradients occur between the plane of focus and the imaging system during and after the preburn event. These localised density gradients result in unpredictable refractive index fluctuations, which may move the focus away from the nominal plane of focus, or significantly disrupt the image collected by the acquisition system. We performed specific experiments to characterise the transient evolution of the depth of field and defocus in our optical setup; the experimental layout and the results are presented and discussed next. Depth of field is commonly measured using a slanted stage micrometer. However, because local variations in focus position and depth of field are expected under the conditions of these experiments, a precision Ronchi ruling was used to characterise the spatial fluctuations of these two parameters. To evaluate these fluctuations in the depth dimension (along the optical axis), the Ronchi ruling was tilted 56.4° away from the imaging plane, while keeping the focus in the centre of the image, as shown in Fig. 5a. Hence the horizontal high-contrast region in Fig. 5a corresponds to the intersection between the slanted Ronchi ruling and the microscope's vertical plane of focus. Based on the magnification
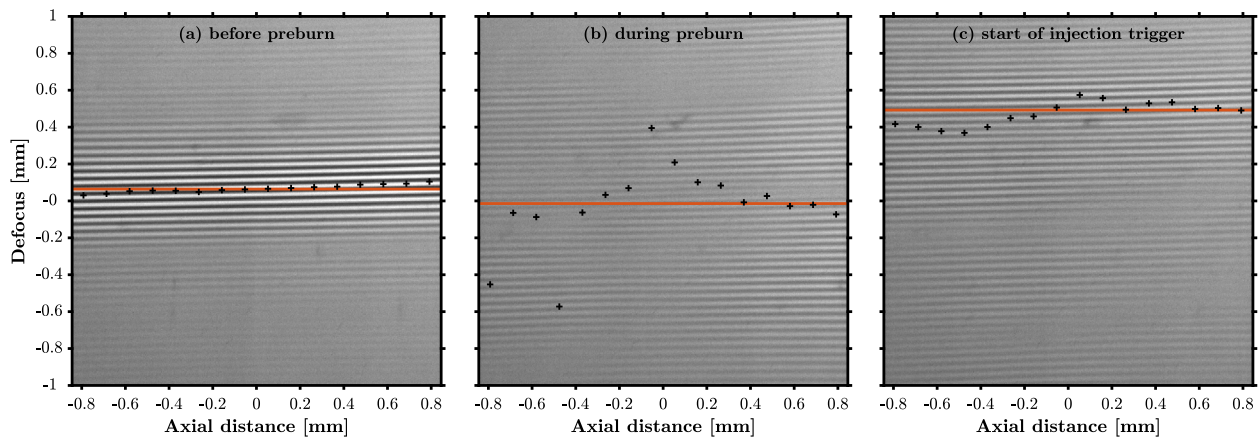

Fig. 5. Ronchi ruling tilted by 56.4° along the optical axis to characterise defocus before preburn (a), during preburn (b), and at the start of injection trigger (c) at ECN Spray A conditions (22.8 kg m^{-3}, 904 K). Crosses indicate the best local focus position, and the red line the estimated defocus across the whole frame. Before preburn the focus is just above mid-frame. During preburn the convective currents inside the vessel introduce significant optical distortions, resulting in randomly focused and defocused regions. At the start of injection trigger the focus has somewhat stabilised but shifted away from the microscope. This figure is also available as **Supplementary video** in the on-line version of this article and on [25], showing the full temporal evolution of the imaging system's defocus during preburn.
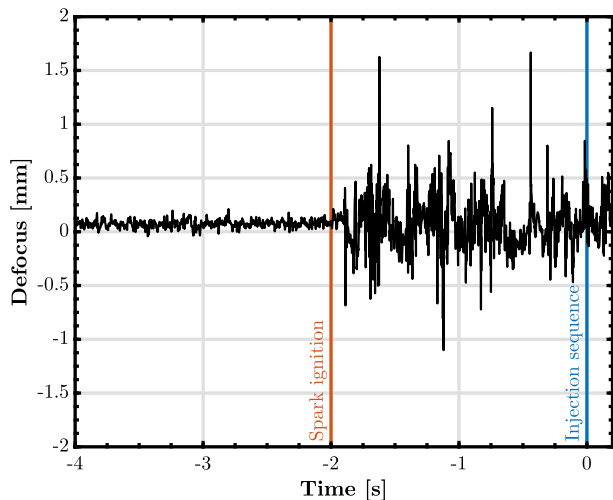
Fig. 6. Defocus as a function of time for Spray A conditions. The timing is relative to the start of injection trigger pulse, with the preburn being initiated by the spark plugs at −2 s, and the sequence of three consecutive injections occurring at 0 s. In-between these two events, refractive index fluctuations cause significant changes to the effective working distance of the microscope, leading to random defocus in excess of ±1 mm.

of our microscope we selected a ruling with a spatial frequency of 20 line pairs per millimetre. This approach enabled us to perform high-speed time-resolved measurements of the optical system's defocus during preburn and cool-down. To quantify the defocus we developed an image processing algorithm which fitted a Gaussian distribution to vertical strips in the images. The black crosses in Fig. 5 indicate the position of the Gaussian's mean, while the red line indicates the estimated defocus across the whole frame. A shortcoming of our approach is that it is intrusive, because inserting such a target plate into the vessel affects both the volume of gas and the surface available for heat transfer. To minimise the extent of this disruption, we customised both the Ronchi ruling and its mounting within the chamber so that their overall volume and surface area were minimal. This experiment showed that significant optical distortions occur during preburn, as the convective currents inside the vessel introduce arbitrarily-oriented refractive index gradients. This results in random microscopic distortions of the plane of focus, as evidenced in Fig. 5b by the fact that several regions along the vertical axis of the Ronchi grating appear simultaneously focused. At the start of injection trigger the focus has somewhat stabilised but shifted away from the microscope (Fig. 5c) by approximately 0.4 mm. The temporal evolution of the defocus is shown in Fig. 6. Our approach to spatially and temporally quantify defocus at the microscopic scale enabled us to better understand the impact of convective currents on the spatial resolution of our imaging system, and how to partially mitigate these effects through an optimisation of the injection timing.

3. Results and discussion

In this section we present evidence that surface tension and primary atomization are significant for *n*-dodecane and *n*-hexadecane when injected into gas up to at least 1200 K, 10 MPa (Section 3.1). We then describe the progression of droplets from *classical evaporation* through a *transitional mixing* regime and towards *diffusive mixing*, as a function of operating conditions (Section 3.2). Finally we demonstrate the effect of fluid properties on this transition (Section 3.3), before summarizing our observations into a reduced pressure–temperature plane and a phenomenological model (Section 3.4).

Any optical measurement of droplets and sprays at transcritical conditions must be interpreted cautiously, taking into account the response of the imaging system and the experimental challenges inherent to such studies. Density gradients across the droplet liquid–gas interface are initially steep, but they progressively relax during droplet heat up [26,14]. Since it is these density gradients that optical imaging captures (shadowgraphy is sensitive to the second spatial derivative of density [27]), one cannot rely solely on a change in interface sharpness as a criterion for supercritical mixing. This optical uncertainty can be significantly compounded by thermal gradients within the pressure vessel, along the optical path of the microscope, which reduce the spatial resolution of the imaging system [18] and lead to artificial blurring of sharp interfaces. We have accounted for these optical uncertainties in the classification of our results by selecting the following three criteria, which had to all be met to support the classification of a droplet transition from evaporation to diffusive mixing:

Criteria 1 Refraction of light can be observed initially, confirming that the liquid/gas interface is sharp and the droplet is in the plane of focus.
Criteria 2 The optical sharpness of the fluid/gas interface degrades *abruptly*, indicating a rapid relaxation of the density gradient across the interface.
Criteria 3 The chunk of fluid is dispersed by local turbulence, rapidly deforming and losing optical density, indicating a mixing process dominated by turbulent and molecular diffusion.

The presence of surface tension was evidenced through the observation of changes in the injected fluid's shape with time: droplets oscillating or deforming elastically, ligaments rotating or breaking to converge into spheres. The temporal evolution of some physical features is a common aspect of all the criteria we employed in our analysis to significantly mitigate the uncertainties that would be found in single-shot, or under-sampled, acquisitions. As such, we note that high-speed imaging to detect the temporal evolution of liquid structure is a critical element of our experimental approach. For these reasons the printed figures cannot convey the full details used in our analysis, and we encourage the reader to consult the video sequences available with the on-line version of this open-access article, and our open-data repository [25].

3.1. Evidence of surface tension and liquid atomization

In order to obtain direct evidence of surface tension and a primary atomization process, we performed systematic measurements with gas temperatures from 700 to 1200 K and densities from 7.6 to 38 kg m^{-3}, corresponding to gas pressures from 2 to 11 MPa. As we will discuss in this section, the experimental results show a transition in behaviour when moving to higher gas temperature and pressure. One example for *n*-hexadecane (Fig. 7a and the associated video in the on-line version of this open access article) shows that surface tension, primary atomization, and a classical evaporation process exist at 38 kg m^{-3} and 907 K (7.9 MPa). The injector's nozzle tip is visible on the left edge of the field of view, with the spray exiting the axially-drilled orifice and penetrating from left to right. No corrections or post-processing was applied to these images, apart from a background intensity normalization, to highlight the quality of the raw results acquired by the imaging system. This image sequence offers a larger field of view than most of the detailed experiments performed in this study, with a visualization window length over 10 mm, providing a digital image scale factor of 11 μm/pixel. This relatively large field of view permits visualizing the spray and its features more completely, while the sufficient resolution of the system allows tracking individual

droplets at the end of injection. While the core of the spray is too dense to optically resolve details, the shear layers at the periphery of the sprays are visibly sharp and free of motion-induced blurring. Small and dispersed individual fuel parcels can be seen entrained by eddies in these shear layers, and appear to remain undisturbed by the air flow. This suggests that they are likely to be dispersed droplets with surface tension, although the scale factor of 11 μm/pixel is too coarse to confirm this by a direct visualization of the liquid/gas interfaces. After the end of injection, the liquid exiting the nozzle breaks up into fluid structures or ligaments,
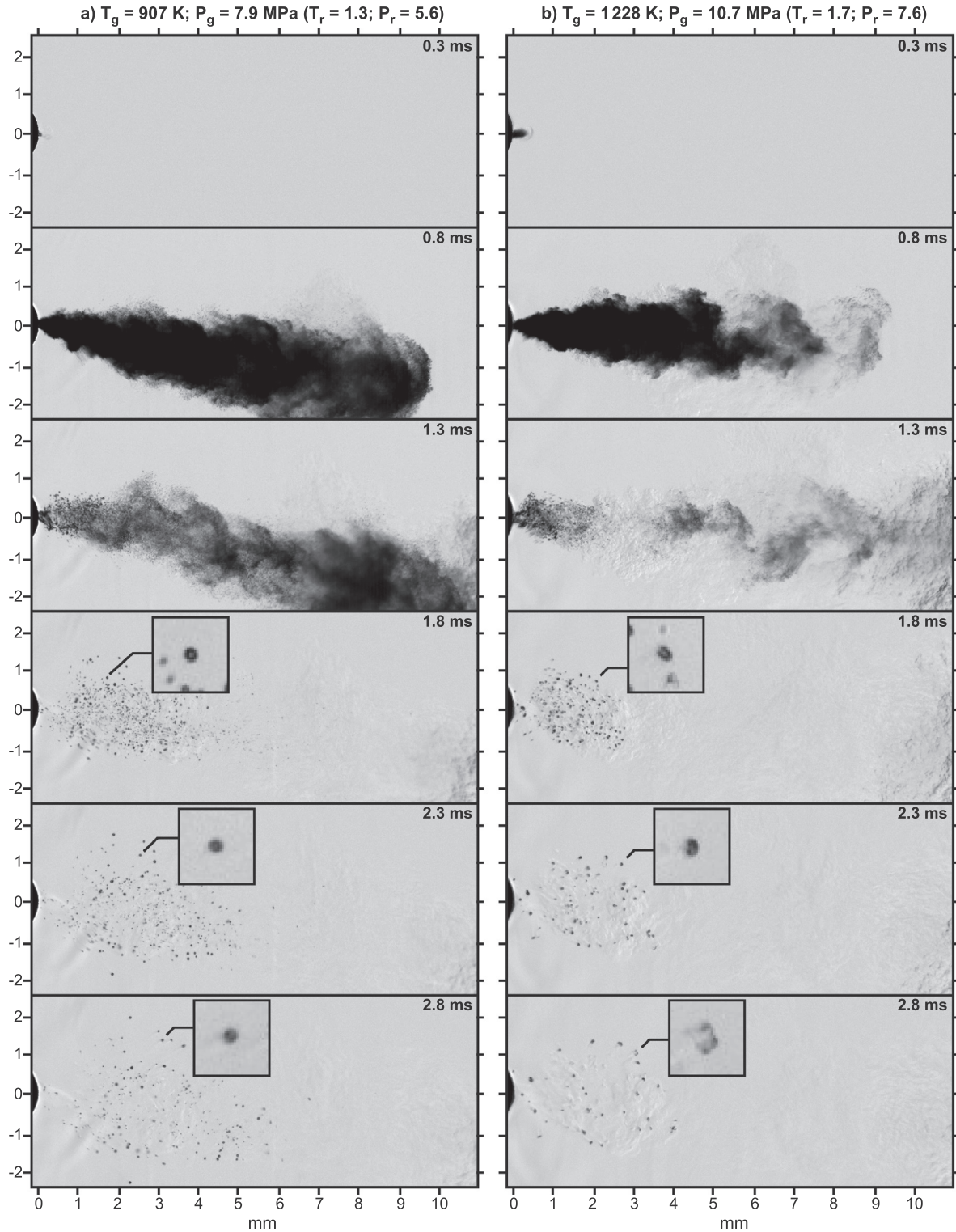

Fig. 7. Injections of *n*-hexadecane into gas at 38 kg m^{-3}. (a) After atomization all droplets converge to spherical shapes, with their diameters progressively reducing. This behaviour is characteristic of a classical evaporation process, even though the conditions are above the critical point of *n*-hexadecane. (b) After atomization most droplets oscillate, remaining non-spherical and abruptly transitioning to vapour phase. At the point of transition the droplets' shape follow a pattern that could be described as a backward-facing bag. The magnified insert represents a 400 μm × 400 μm field of view. A video of this and 2 subsequent injections is available on-line [25].

which quickly disintegrate into many droplets, all converging to spherical shapes. These droplets are and remain spherical throughout the event, manifesting the significant influence of surface tension on the fluid at this condition. The magnified region in Fig. 7a tracks the evolution of a single droplet at the end of injection over a 400 µm × 400 µm field of view. Fig. 7a illustrates that droplets initially exhibit a sharp interface and refraction of light through their centres. The droplets remain spherical for over a millisecond, reducing progressively in size until they are no longer detected by our instrument, shortly before complete evaporation. This behaviour is characteristic of a classical (i.e. subcritical) evaporation process, even though this measurement was performed under ambient conditions well above the nominal critical point of n-hexadecane ($T_r = 1.3$ and $P_r = 5.6$).

To investigate the presence of atomization and surface tension at more elevated operating conditions, we increased the gas temperature to 1228 K while maintaining the gas density at 30.4 kg m^{-3} (resulting in a gas pressure of 10.7 MPa prior to injection). The temporal evolution of a spray of n-hexadecane injected into that environment (Fig. 7b) shows that again, the core of the spray is too optically dense to resolve details but the shear layers at the periphery of the sprays remain sharp and free of motion blurring. The shear layers contain fewer discrete fuel parcels than in the 907 K case (Fig. 7a), indicating a more rapid mixing and evaporation of the fuel with the ambient gas. The liquid exiting the nozzle at the end of injection breaks up into a multitude of ligaments and droplets of different diameters. Stretched ligaments rotate and rapidly converge into spheroidal droplets (e.g. at 10 ms after start of recording on Video 2 in the on-line version of this article). The dispersed droplets then oscillate as they penetrate through the ambient gas. The oscillation of these droplets indicates that surface tension is weak but certainly existent. From these direct observations we can conclude that even under such elevated conditions ($T_r = 1.7$ and $P_r = 7.6$) surface tension and primary atomization are present and significant in the near nozzle region. But remarkably, and in stark contrast to the lower temperature case, the droplets *do not* continue to follow a classical evaporation process with a progressive reduction in diameter until disappearance. Instead the magnified region in Fig. 7b shows that droplets abruptly deform or expand, transitioning into an optically dense fluid that stretches and rapidly mixes with the ambient gas with little or no evidence of surface tension. To the best of our knowledge, the high-speed microscopy performed in this study at elevated T_r and P_r presents the first direct evidence that surface tension and primary atomization remain important features of diesel mixing, and that there is also a transition to a miscible state with little surface tension.

3.2. Droplet transition from classical evaporation to diffusive mixing

Our observations confirm that two-phase classical evaporation is a significant feature of diesel spray mixing, even at ambient gas conditions nominally above the fuel's critical point (Fig. 7a). Our measurements also show that at ambient conditions significantly above the fuel's critical point, classical evaporation still occurs for some time but it is abruptly superseded by a single-phase two-fluid diffusive mixing process (Fig. 7b). In order to develop and verify physically accurate models, it is now essential to investigate the mechanics of this transient phenomenon at the microscopic scale. In doing so, we will show that the time taken by droplets to transition into a dense fluid is not negligible compared to typical durations or timescales for diesel injection. Having established that the transition from droplet evaporation to diffusive mixing has a finite duration, we will first describe the process and timescale of this transition for n-dodecane as a function of gas temperature and pressure. In Section 3.3 we will then consider the effect that the fuel's properties have on the time taken for the transition to occur, and on the subsequent deformation of the fuel parcels.

To demonstrate the effect of operating conditions on the evolution of individual droplets, we recorded high-speed videos with a spatial scale of 2.5 µm/pixel and extracted 300 µm × 300 µm regions centred on moving droplets (Fig. 8). The gas density was 38 kg m^{-3} and the target gas temperatures were 700, 1000 and 1200 K, resulting in pressures of 6.2, 8.8 and 10.6 MPa, respectively.

The droplet injected into 700 K gas travels at 0.2 m s^{-1} and exhibits a continuous reduction in diameter, with no noticeable change in droplet shape, demonstrating a classical evaporation and mixing even though the gas temperature and pressure are above the critical point of n-dodecane. This can be explained by the fact that the time required to completely evaporate the droplet is shorter than the time required for the droplet to transition to a supercritical fluid. During this time, adiabatic mixing arguments
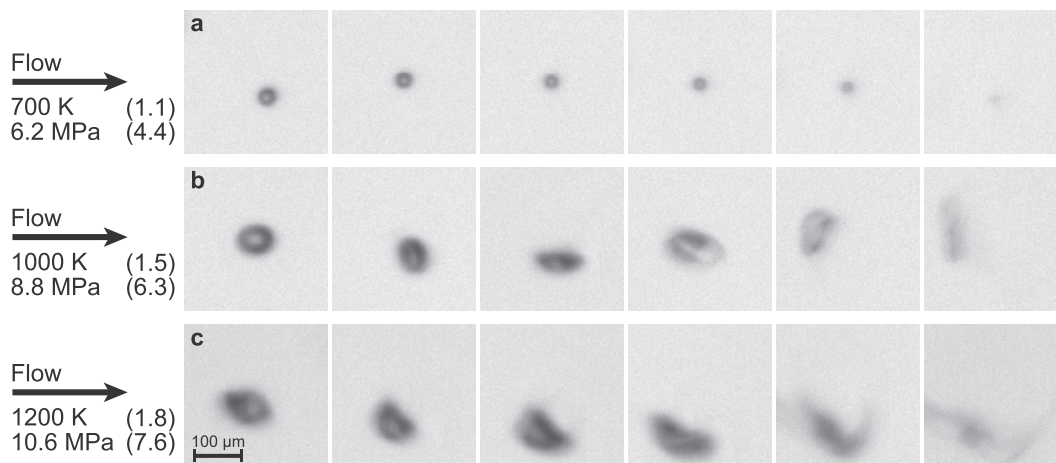

Fig. 8. Evolution of individual n-dodecane droplets into gas at 30.4 kg m^{-3}, as a function of ambient pressure and temperature. Each image represents a 300 µm × 300 µm field of view centred on the moving droplet. The figures in brackets indicate the reduced temperatures (T_r) and pressures (P_r). (**a**) The droplet remains spherical with a continuous reduction in diameter, indicating a classical evaporation process. (**b**) Deformations occur before disintegration is initiated at the wake side of the droplet. (**c**) Significant deformations occur before the fuel appears to stretch and diffuse, readily mixing with the surrounding gas without evidence of surface tension. The video is available on-line [25].
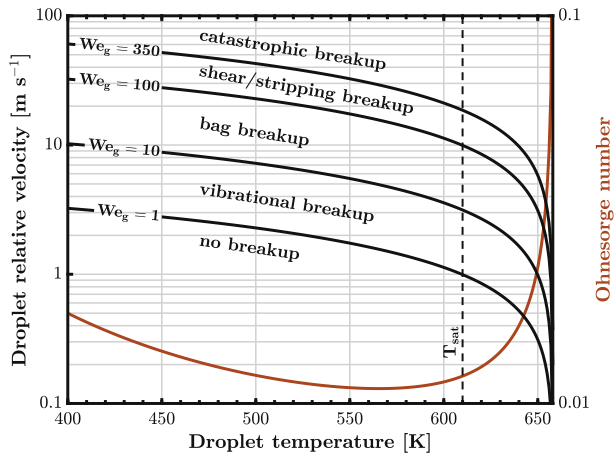
Fig. 9. Secondary atomization regimes for a 50 μm droplet of *n*-dodecane into gas at 30.4 kg m^{-3}. The Ohnesorge number is below 0.1 for all subcritical temperatures, indicating that the breakup mode boundaries should be valid and only depend on the Weber number. The dotted line shows the saturation temperature for an *n*-dodecane/nitrogen mixture at equilibrium under these conditions, computed based on [10]. The plot indicates that droplets travelling at 1 m s^{-1} into 30.4 kg m^{-3} gas (e.g. droplets in Fig. 8) may just reach a vibrational breakup regime before reaching the saturation temperature, but attaining the bag breakup regime would require droplets to be at temperatures significantly above T_{sat}, which cannot be achieved in a classical evaporation regime.

suggest that the droplet temperature remains lower than the critical temperature.

The droplet injected into 1000 K gas exhibits a qualitatively different behaviour. It was captured 5 mm downstream from the nozzle orifice, and initially displays a sharp interface and a bright refraction spot in its centre, indicating that the droplet is in a liquid state (i.e. with significant surface tension). We can observe that this droplet rapidly deforms and we deduce that its surface tension is likely diminished compared to that of the droplet injected into 700 K. After an initial deformation the droplet's refraction spot disappears, but the droplet's interface remains sharp throughout the sequence. This apparent sharpness suggests that a liquid–gas interface persists, and that the droplet may experience the beginning of an aerodynamic breakup process. It is notable that the initiation of this disintegration process takes place at the *wake side* of the droplet, and results in a backward-facing bag. This was a

particularly frequent and consistent feature in our observations of *n*-dodecane droplet disintegration at elevated pressures and temperatures. Interestingly, this behaviour agrees with observations [28] and simulations [29,30] for the disintegration of transcritical liquid oxygen (LOX) droplets in gaseous hydrogen. Such progressive deformation of droplets into backward-facing bag is a viscous phenomenon attributed to the formation of a recirculating eddy in the wake region [31], which increases the pressure distribution over the rear of the droplet [29,30]. In our experiment this disintegration did not produce visible secondary droplets, or ligaments connecting these droplets. While we cannot exclude the possibility that secondary droplets would be too small to be resolved by our optical instrument, it is also possible that the heating rate of the primary droplet would increase significantly during the deformation associated with secondary atomization, producing non-uniformity in temperature and surface tension. While the final images appear diffusive, it cannot be ascertained from this video whether the final vaporisation mechanism followed a classical evaporation, or a two-fluid diffusive mixing process. This sudden deformation and increase in surface area could be sufficient to increase convective mixing, and expedite the complete vaporisation of the liquid fuel [30].

Finally, the 1 200 K case also shows significant deformation of the fuel droplet, but its initially sharp interface rapidly becomes diffuse (Fig. 8c). Shortly after the beginning of the video sequence the fuel appears to stretch and diffuse, readily mixing with the surrounding gas without evidence of surface tension. The mixing that ensues could be described as a single-phase two-fluid diffusive mixing process, between fluids of different densities. In this case, spatial gradients in density persist to make the fuel appear somewhat optically dense until these gradients are reduced through diffusive mixing. While the timescale for transition to purely diffusive mixing will certainly depend upon the local droplet diameter, convective flow, and exposure to surrounding fuel vapour and mixture temperature, the time taken for this particular 60 μm droplet to transition into what appears to be a 'supercritical' fluid is on the order of 1 ms. This timescale is significant compared to spray mixing timescales, or to a typical injection duration used for diesel injections.

We could not measure the droplets' temperatures and therefore estimate the physical properties of the liquid phase. This makes it impossible to accurately derive parameters such as the Weber and Ohnesorge numbers, which would otherwise aid the interpretation
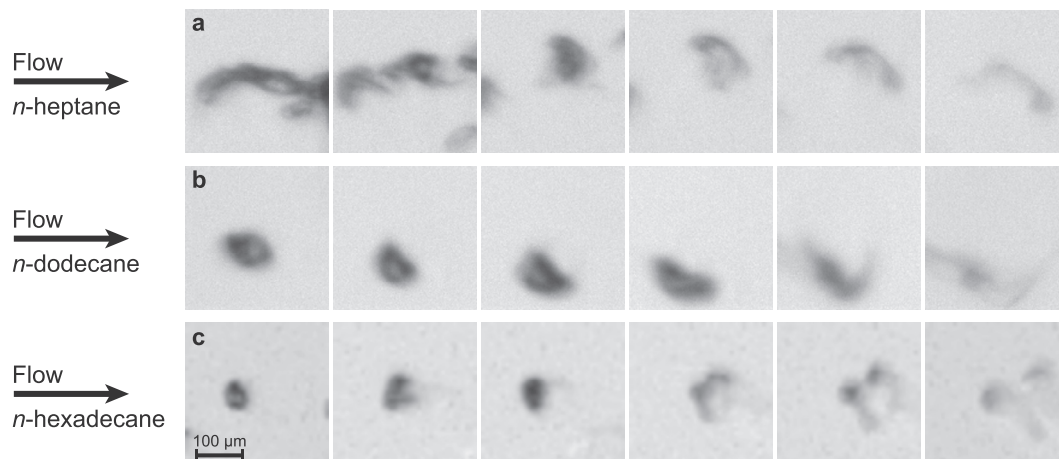

Fig. 10. Evolution of individual droplets into gas at 30.4 kg m^{-3} (1200 K, ≈ 10.6 MPa) as a function of fuel type. Each image represents a 300 μm × 300 μm field of view centred on the moving droplet. (**a**) *n*-heptane follows a diffusive mixing process from the nozzle's exit throughout the video sequence. (**b**) The *n*-dodecane droplet deforms until stretching and diffusing with the surrounding gas with no further evidence of surface tension. (**c**) The *n*-hexadecane droplet experiences significant oscillations before transitioning into a dense fluid from the wake side. The video is available on-line [25].

of our measurements. However, knowing the physical properties of n-dodecane [32] we can compute these parameters as a function of droplet temperature and velocity. Hence we can plot the expected atomization modes in a velocity–temperature domain (Fig. 9) to compare with our measurements and make two observations. First, the Ohnesorge number is small ($Oh < 0.1$) for all subcritical temperatures, indicating that the boundaries for secondary atomization regimes should be valid and only dependent on the Weber number [33]. Second, the gaseous Weber number for droplets travelling at $1\,m\,s^{-1}$ into $30.4\,kg\,m^{-3}$ gas (e.g. droplets in Fig. 8) is particularly small ($We_g \approx 1$). Hence these droplets travelling at $1\,m\,s^{-1}$ should remain stable until they heat up to approximately 610 K which happens to be the intersection between the saturation temperature (T_{sat}) and the vibrational breakup regime transition ($We_g = 1$). Depending on the exact conditions, some of these droplets may just reach a vibrational breakup regime before reaching the saturation temperature, but attaining the bag breakup regime would require droplets to be at temperatures significantly above T_{sat}, which cannot be achieved in a classical evaporation regime. The evolution of the droplets' shapes in Fig. 8 are in good qualitative agreement with these observations. Whilst Fig. 9 could explain the lack of oscillation for the droplet injected into 700 K gas and the more significant deformations for the droplet injected into 1000 K gas, it does not provide an explanation for the disintegration processes of the droplets injected into 1000 K and 1200 K gas, but it confirms that the backward-facing bag disintegration is in no way related to the classical bag breakup regime. We can conclude from this analysis that the mechanisms being observed cannot be described by the well-known secondary breakup regimes that have been extensively studied under isothermal conditions.

3.3. Effect of fluid properties on droplet transition

To examine the effect of the fuel's properties on the vaporisation mechanism, or the transition to supercritical fluid at elevated pressures and temperatures, we show another video sequence in Fig. 10 to compare the behaviour of n-heptane, n-dodecane and n-hexadecane. The spatial scale is also 2.5 μm/pixel and the regions centred on moving droplets represent 300 μm × 300 μm. The gas density was $30.4\,kg\,m^{-3}$ and the target gas temperature was 1200 K in all cases, resulting in a pressure of 10.6 MPa. In the case of n-heptane the fuel follows a diffusive mixing process throughout the video sequence. This is particularly remarkable due to the fact that this video sequence occurs within the first 500 μm of the nozzle exit, which corresponds to less than 3 nozzle diameters downstream. Hence at these conditions n-heptane showed no signs of significant surface tension, and appeared to rapidly transition into a supercritical fluid. This behaviour is displayed in more detail in Fig. 11.

The n-dodecane sequence is identical to the one from Fig. 8, and described earlier. This 60 μm droplet transitions into a chunk of supercritical fluid, which mixes with the surrounding gas through a single-phase two-fluid mixing process.

The n-hexadecane droplet in Fig. 10 exhibits a different behaviour to those of n-heptane and n-dodecane. This sequence shows that the liquid droplet initially experiences noticeable deformations, demonstrating a small but significant surface tension. The droplet then follows a disintegration process initiated at the wake side of the droplet. This is in some way comparable to the disintegration observed in Fig. 10 for the 1000 K case, but the n-hexadecane droplet disintegrates into three separate chunks of fluid that resemble a ring and spheroid. This behaviour was particularly consistent for n-hexadecane, but not observed for the other two fuels used in our study. This suggests that the physical properties of the fuel have a significant effect on both the timescale
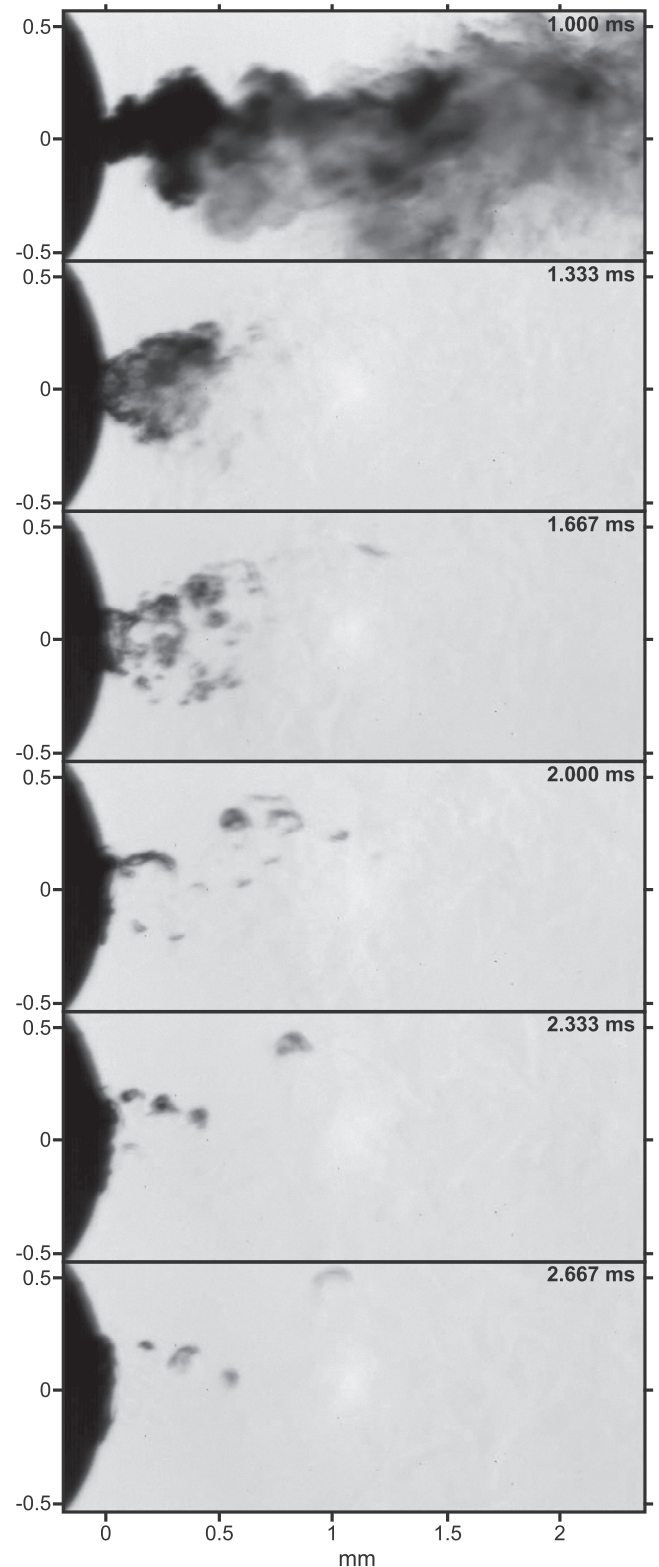

Fig. 11. The end of injection for n-heptane at $30.4\,kg\,m^{-3}$, 1198 K (10.4 MPa). At these extreme conditions surface tension appears inexistent and a traditional atomization process cannot be observed. Diffusive mixing seems to take place from the nozzle outlet, indicating a supercritical injection process. A video of this spray is available on-line [25].

and the mechanism of disintegration and transition into supercritical fluid. A detailed investigation of the causes for these different behaviours is needed, but beyond the scope of this article.
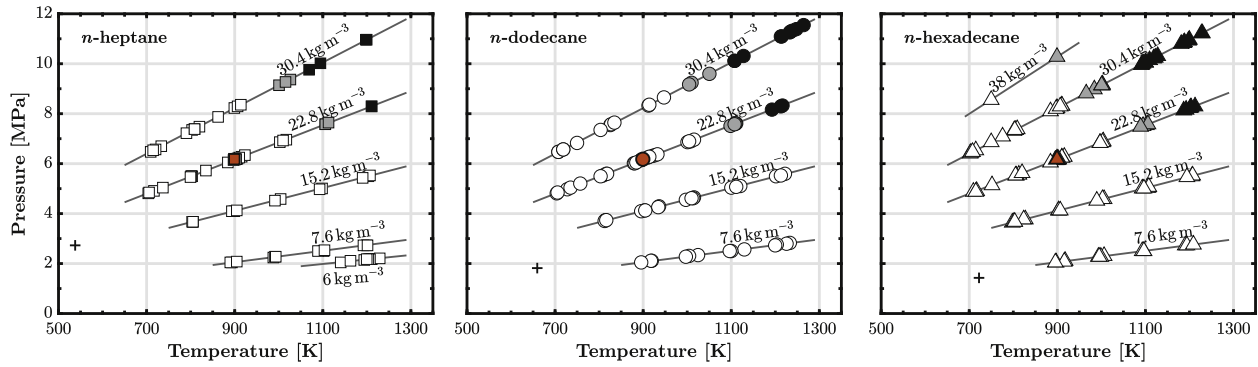
Fig. 12. Gas pressure–temperature diagrams showing our classification of mixing regimes for each fuel. Red symbols indicate the ECN Spray A test condition (22.8 kg m^{-3}, 900 K). White symbols represent a *classical evaporation* regime where droplets remain spherical and exhibit a progressive mass transfer. Grey symbols indicate a *transitional mixing* regime where droplets show evidence of a reduced surface tension, with significant stretching and deformation of the liquid/gas interface leading to an accelerated mixing. Black symbols identify a *diffusive mixing* regime where atomization and surface tension may be observed initially but fuel parcels rapidly transition into chunks of supercritical fluids with a mixing regime dominated by diffusion and convection, and an evident disappearance of surface tension.

A classification of our observations as pressure–temperature diagrams for *n*-heptane, *n*-dodecane and *n*-hexadecane is presented in Fig. 12. We observe that the mixing regime boundaries are not significantly different for these three fluids in the (P_g, T_g) plane. The mapping shows that for all three alkanes, diffusive mixing was only observed in regions of the pressure–temperature diagram significantly above the critical point of the fuel. This classification indicates that the exact conditions where diffusive mixing occurs are mainly function of the gas pressure and temperature with little sensitivity to the fluids' properties for the range of alkanes considered, although as noted previously the physical properties of the fuel have a rather significant effect on both the timescales and the morphology of the droplets' disintegration and transition into supercritical fluid.

3.4. Phenomenological model

We present in Fig. 13 a classification of all our observations in a reduced pressure–temperature plane. One should stress that presenting these data into a set of (P_r, T_r) plane and correlations with respect to the fuel single-component critical properties is simply a convenient means of reducing our dataset for general comparison with other studies; it is not an implication that reduced pressures and temperatures are the key parameters behind the physics of transcritical mixing regimes. We performed an automated classification of our dataset using the least squares solution for an arbitrary regression model in the form $T_r^n \times P_r^m = C$. Reasonable fits were found for $n \approx 1$ and $m \approx 0.5$, hence we chose to present the correlations in the form $T_r \sqrt{P_r}$, with different values for the constant C for each mixing regime transition. These three mixing regimes are illustrated in Fig. 14 and categorised as follows:

Fig. 13. Classification of the mixing regimes for all the experimental conditions. Both P_r and T_r are calculated by dividing the imposed far-field (P_g, T_g) values by the critical values of the fuel (P_c, T_c). White symbols represent test conditions where classical evaporation is observed, with droplets remaining spherical throughout their lifetime. Grey symbols indicate conditions where droplets undergo a transitional mixing with evidence of surface tension but significant droplet stretching and deformation, leading to an accelerated mixing. Black symbols indicate conditions where surface tension may be observed initially but the droplets rapidly transition to a mixing regime dominated by diffusion, with no more evidence of surface tension. The red symbols indicate the standard ECN Spray A test conditions (22.8 kg m^{-3}, 900 K, ≈ 6 MPa) for each alkane. The area highlighted in grey illustrates an envelope of conditions relevant to the injection of a multi-component fuel into a modern diesel engine ($P_g \approx 4 - 11$ MPa, $T_g \approx 800 - 1000$ K, $P_c = 2.2$ MPa, $T_c = 720$ K).

Regime I – Classical evaporation

Droplets in this regime follow the well-known atomization and evaporation processes characterised by significant surface tension, continuous and progressive heat and mass transfer between a liquid phase and a gaseous phase. The droplets show little, if any, departure from the spherical shape throughout their lifetime. When subjected to a turbulent flow field these droplets may deform and change trajectory, but they do not abruptly diffuse with the surrounding gas. The normal alkanes used in this study exhibit this mixing regime over the space $T_r \sqrt{P_r} \leqslant 3.3$ on the interval $\{T_r \in [1, 2.3]\} \cap \{P_r \in [0.7, 8]\}$.
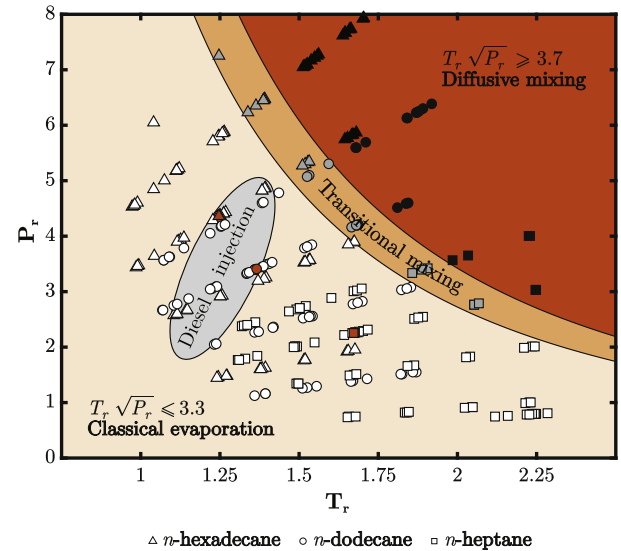
Regime II – Transitional mixing

Droplets undergo a mixing regime which is initially dominated by classical atomization and evaporation processes but then exhibit a significantly accelerated vaporisation. This regime is characterised by a rapid reduction of intermolecular forces. Droplets deform and oscillate continuously, thus accelerating their rate of heating and vaporisation, until surface tension is no longer sufficient to overcome the aerodynamic forces. This leads to a catastrophic stretching of the liquid/gas interface initiated at the wake side of the droplet, followed by a rapid vaporisation of the whole droplet. The initiation of disintegration at the wake indicates that the
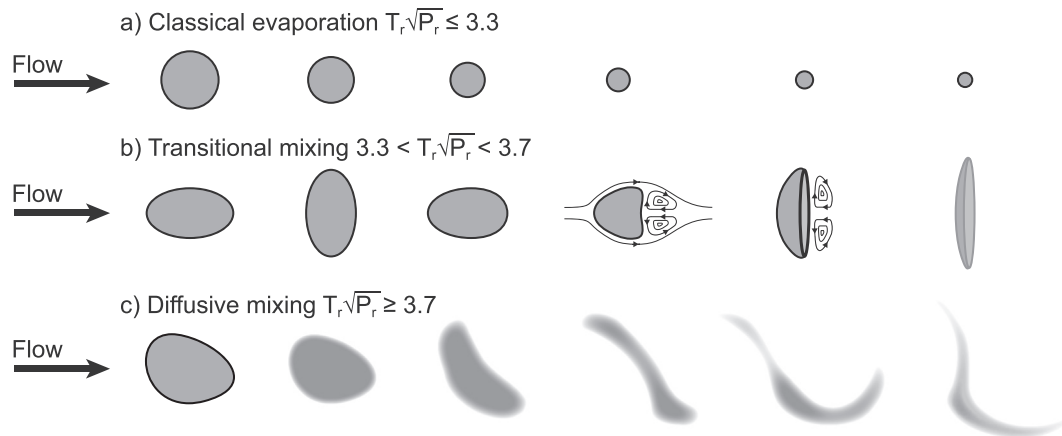
a) Classical evaporation $T_r\sqrt{P_r} \leq 3.3$

Flow

b) Transitional mixing $3.3 < T_r\sqrt{P_r} < 3.7$

Flow

c) Diffusive mixing $T_r\sqrt{P_r} \geq 3.7$

Flow

Fig. 14. Conceptual model of droplet mixing regimes. *Classical evaporation* is a significant feature of fuel spray mixing, even at ambient gas conditions nominally above the fuel's critical point. *Transitional mixing* is characterised by a rapidly diminished surface tension. Droplet disintegration is initiated at the wake side, resembling a backward-facing bag due to the formation of a recirculating eddy. *Diffusive mixing* in transcritical regime may initially include a liquid/gas interface, although droplets cannot be assumed spherical as they deform continuously. The fuel rapidly transitions to a single-phase mixing regime dominated by interdiffusion and convection, with no evidence of elastic interfaces. The optically-dense chunks of supercritical fluid diffuse with the surrounding gas and mix through small-scale turbulence.

droplets' interface could be subjected to instabilities due to recirculation vortices near the rear stagnation point [34]. This process is likely to be accelerated by the thermal Marangoni (thermocapillary) effect which causes the trailing edge of the droplet to be hotter than the leading edge [35], resulting in diminished surface tension forces at the wake. One should note that multi-component fuels may show an additional solutal Marangoni (diffusocapillary) effect [36]. It is not possible to ascertain from our experimental data if the final vaporisation follows a classical evaporation process accelerated by a deformed liquid/gas interface, or a transition from liquid droplet into a chunk of supercritical fluid. Although the underlying physical process could not be fully resolved it should be remarked that the final gasification is completed in less than 0.5 ms, hence from a practical standpoint the assumption of a deformed two-phase interface may adequately capture the mixing time scales. In this study normal alkanes were found to exhibit a transitional mixing regime over the space $3.3 < T_r\sqrt{P_r} < 3.7$ on the interval $\{T_r \in [1, 2.3]\} \cap \{P_r \in [0.7, 8]\}$.

Regime III – Diffusive mixing
The injected fuel may initially exhibit clear evidence of surface tension through the stretching of liquid/gas interfaces and the refraction of light. Droplets cannot be assumed spherical in shape as they oscillate and deform continuously. The assumption of a two-phase flow can only be valid for very short time scales and cannot accurately describe the full mixing process. The fuel rapidly transitions to a single-phase mixing regime dominated by interdiffusion and convection, with no evidence of elastic interfaces. When subjected to a turbulent flow field the optically-dense chunks of supercritical fluid readily diffuse with the surrounding gas. The normal alkanes used in this study were found to exhibit a diffusive mixing regime over the space $T_r\sqrt{P_r} \geq 3.7$ for the interval $\{T_r \in [1, 2.3]\} \cap \{P_r \in [0.7, 8]\}$.

4. Conclusions

We performed systematic measurements using high-speed high-resolution microscopic visualizations, for three single-component fuels (*n*-heptane, *n*-dodecane, *n*-hexadecane) into inert gaseous environments at temperatures from 700 to 1 200 K and pressures from 2 to 11 MPa. We summarised our observations into a phenomenological model which describes the morphological evolution of microscopic droplets before, during, and after their transition from evaporation to diffusive mixing. We provide criteria for these transitions as pressure–temperature charts, revealing the conditions where transcritical mixing is important to diesel fuel spray mixing. Significant findings from this study include:

1. We found clear evidence of surface tension and primary atomization at all these conditions for *n*-dodecane and *n*-hexadecane during some stages of injection. We also observed clear evidence of surface tension for *n*-heptane, except under the most elevated conditions (1200 K, 10 MPa) where diffusive mixing appeared to take place at the nozzle exit.
2. *Classical evaporation* is a significant feature of fuel spray mixing, even at ambient gas conditions nominally above the fuel's critical point. Both classical atomization and evaporation were observed over the space $T_r\sqrt{P_r} \leqslant 3.3$, for the interval $\{T_r \in [1, 2.3]\} \cap \{P_r \in [0.7, 8]\}$.
3. *Transitional mixing* is an intermediate mixing regime characterised by a fast heating of the liquid fuel, leading to a rapidly diminished but non-negligible surface tension. A characteristic feature of this regime is a disintegration at the wake side of the moving droplet, suggesting the presence of a vortical wake and non-homogeneous internal temperature and surface tension fields, followed by a prompt vaporisation of the deformed liquid. This process indicates that a different secondary breakup regime occurs when the liquid and gas phases have significantly different temperatures. To the best of our knowledge this type of non-isothermal droplet disintegration process has not been extensively studied despite its relevance to combustion systems and cryogenic sprays.
4. *Diffusive mixing* was observed for the first time for operating conditions, temporal and spatial scales representative of combustion engines. Continuously deforming liquid droplets may initially exist before they transition into chunks of supercritical fluid. The time taken by a droplet to transition to diffusive mixing depends on both the fuel properties and the gas pressure and local temperature. This transcritical process was found to occur when gas pressures and temperatures simultaneously exceed ≈ 8 MPa and ≈ 1100 K ($T_r\sqrt{P_r} \geqslant 3.7$ for the interval $\{T_r \in [1, 2.3]\} \cap \{P_r \in [0.7, 8]\}$).

Our measurements provide new evidence of the evolution of fuel mixing at the microscopic scale under harsh, high temperature

and pressure conditions, and the influence of fuel type and operating conditions on this process. These findings provide new evidence that can be used by modellers to justify accounting for, or neglecting, liquid breakup and evaporation processes in their models. These new experimental data open the way to the development of more complete phenomenological and physical models for transcritical mixing, and enable a direct and systematic verification of numerical models. Hence there is a wide scope for further studies, both experimental and numerical, and we suggest that future efforts should be focused on:

- Validating models for transcritical droplet disintegration. In the absence of quantitative measurements of droplet temperature, a qualitative validation could be done based on the temporal evolution of droplet shapes, as a function of operating conditions and fuel type.
- Extending this phenomenological model to smaller and faster droplets. While the range of droplet sizes we observed is relevant to heavy duty diesel engines, the fuel sprays in light duty combustion systems are known to generate significantly smaller droplets during the main injection. By increasing the optical magnification nearer to the diffraction limit it may be possible to observe the deformation and transition of smaller and faster droplets present in the shear layers at the periphery of the spray.
- Measuring droplet temperature during its heating up phase. One approach would be to use optical diagnostics that can accurately measure refractive index, from which the droplet temperature can then be inferred. Rainbow refractometry may be able provide such information [37,38], at least while droplets are close to the spherical shape.
- Characterizing the disintegration and mixing of multicomponent fuels. The normal alkanes used in this fundamental study showed similar mixing regime boundaries in both the (P_g, T_g) and (P_r, T_r) planes, although they showed different transition timescales and droplet morphologies. The transport and thermodynamic properties of these alkanes are different to those of complex fuels such as diesel and kerosene, hence a key question that arises from our work is: Do multicomponent fuels follow the same transition pathways and timescales as these alkanes?

Videos and data presented in this article are openly available from the University of Brighton data archive at https://doi.org/58P [25].

Acknowledgements

References

[1] Bellan J. Supercritical (and subcritical) fluid behavior and modeling: drops, streams, shear and mixing layers, jets and sprays. Prog Energy Combust Sci 2000;26(4–6):329–66. http://dx.doi.org/10.1016/S0360-1285(00)00008-3.

[2] Dahms RN. Understanding the breakdown of classic two-phase theory and spray atomization at engine-relevant conditions. Phys Fluids 2016;28(4):042108. http://dx.doi.org/10.1063/1.4946000.

[3] Morin C, Chauveau C, Dagaut P, Gokalp I, Cathonnet M. Vaporization and oxidation of liquid fuel droplets at high temperature and high pressure: application to n-alkanes and vegetable oil methyl esters. Combust Sci Technol 2004;176(4):499–529. http://dx.doi.org/10.1080/00102200490276719.

[4] Weckenmann F, Bork B, Oldenhof E, Lamanna G, Weigand B, Dreizler A. Single acetone droplets at supercritical pressure: droplet generation and characterization of PLIFP. Zeitschrift für Physikalische Chemie International Journal of Research in Physical Chemistry and Chemical Physics 2011;225(11–12):1417. http://dx.doi.org/10.1524/zpch.2011.0188.

[5] Winter M, Melton LA. Measurement of internal circulation in droplets using laser-inducedfluorescence. Appl Opt 1990;29(31):4574–7. http://dx.doi.org/10.1364/AO.29.004574.

[6] Falgout Z, Rahm M, Wang Z, Linne M. Evidence for supercritical mixing layers in the ECN Spray A. Proc Combust Inst 2015;35(2):1579–86. http://dx.doi.org/10.1016/j.proci.2014.06.109.

[7] Falgout Z, Rahm M, Sedarsky D, Linne M. Gas/fuel jet interfaces under high pressures and temperatures. Fuel 2016;168:14–21. http://dx.doi.org/10.1016/j.fuel.2015.11.061.

[8] Wensing M, Vogel T, Götz G. Transition of diesel spray to a supercritical state under engine conditions. Int J Engine Res 2016;17(1):108–19. http://dx.doi.org/10.1177/1468087415604281.

[9] Manin J, Bardi M, Pickett LM, Dahms RN, Oefelein JC. Microscopic investigation of the atomization and mixing processes of diesel sprays injected into high pressure and temperature environments. Fuel 2014;134:531–43. http://dx.doi.org/10.1016/j.fuel.2014.05.060.

[10] Siebers DL. Scaling liquid-phase fuel penetration in diesel sprays based on mixing-limited vaporization, SAE J Eng 108(3). http://dx.doi.org/10.4271/1999-01-0528.

[11] Chehroudi B, Talley D, Coy E. Visual characteristics and initial growth rates of round cryogenic jets at subcritical and supercritical pressures. Phys Fluids 2002;14(2):850–61. http://dx.doi.org/10.1063/1.1430735.

[12] Chehroudi B, Cohn R, Talley D. Cryogenic shear layers: experiments and phenomenological modeling of the initial growth rate under subcritical and supercritical conditions. Int J Heat Fluid Flow 2002;23(5):554–63. http://dx.doi.org/10.1016/S0142-727X(02)00151-0.

[13] Dahms RN, Oefelein JC. On the transition between two-phase and single-phase interface dynamics in multicomponent fluids at supercritical pressures. Phys Fluids 2013;25(9):092103. http://dx.doi.org/10.1063/1.4820346.

[14] Dahms RN, Oefelein JC. Non-equilibrium gas-liquid interface dynamics in high-pressure liquid injection systems. Proc Combust Inst 2015;35(2):1587–94. http://dx.doi.org/10.1016/j.proci.2014.05.155.

[15] Dahms RN, Manin J, Pickett LM, Oefelein JC. Understanding high-pressure gas-liquid interface phenomena in diesel engines. Proc Combust Inst 2013;34(1):1667–75. http://dx.doi.org/10.1016/j.proci.2012.06.169.

[16] Crua C, Shoba T, Heikal MR, Gold MR, Higham C. High-speed microscopic imaging of the initial stage of diesel spray formation and primary breakup, SAE Technical Paper 2010-01-2247; 2010. http://dx.doi.org/10.4271/2010-01-2247.

[17] Shoba T, Crua C, Heikal MR, Gold MR. Optical characterisation of diesel, RME and kerosene sprays by microscopic imaging. In: 24th ILASS-Europe, Estoril, Portugal, 5–7 Sep 2011. URL http://ilasseurope.org/publications/proceedings/.

[18] Crua C, de Sercey G, Heikal MR. Dropsizing of near-nozzle diesel and RME sprays by microscopic imaging. In: 12th ICLASS, Heidelberg, Germany; 2–6 Sep 2012. URL http://ilasseurope.org/publications/proceedings/.

[19] Crua C, de Sercey G, Gold M, Heikal M. Image-based analysis of evaporating diesel sprays in the near-nozzle region. In: 25th ILASS-Europe, Crete, Greece; 1–9 Sep 2013. URL http://ilasseurope.org/publications/proceedings/.

[20] Crua C, Heikal MR, Gold MR. Microscopic imaging of the initial stage of diesel spray formation. Fuel 157. https://doi.org/4F3.

[21] Pickett LM, Genzale CL, Bruneaux G, Malbec L-M, Hermant L, Christiansen C, Schramm J. Comparison of diesel spray combustion in different high-temperature, high-pressure facilities. SAE Int J Engines 2010;3(2):156–81. http://dx.doi.org/10.4271/2010-01-2106.

[22] Meijer M, Somers B, Johnson J, Naber J, Lee S-Y, Malbec LM, Bruneaux G, Pickett LM, Bardi M, Payri R, Bazyn T. Engine combustion network (ECN): characterization and comparison of boundary conditions for different combustion vessels. Atomization Sprays 2012;22(9):777–806. http://dx.doi.org/10.1615/AtomizSpr.2012006083.

[23] Williams CS, Becklund OA. Introduction to the optical transfer function. In: Wiley Series in Pure and Applied Optics. New York: Wiley; 1989.

[24] ISO 12233:2014(E), Photography – electronic still picture imaging – resolution and spatial frequency responses.

[25] Crua C, Manin J, Pickett LM. On the transcritical mixing of fuels at diesel engine conditions 2017. http://dx.doi.org/10.17033/DATA.00000029. URL https://doi.org/58P.

[26] Harstad K, Bellan J. Isolated fluid oxygen drop behavior in fluid hydrogen at rocket chamber pressures. Int J Heat Mass Transfer 1998;41(22):3537–50. http://dx.doi.org/10.1016/S0017-9310(98)00049-0.

[27] Settles GS. Schlieren and shadowgraph techniques. In: Experimental Fluid Mechanics. Berlin Heidelberg: Springer; 2001. http://dx.doi.org/10.1007/978-3-642-56640-0.

[28] Mayer WOH, Schik AHA, Vielle B, Chauveau C, Gökalp I, Talley DG, Woodward RD. Atomization and breakup of cryogenic propellants under high-pressure subcritical and supercritical conditions. J Propul Power 1998;14(5):835–42. http://dx.doi.org/10.2514/2.5348.

[29] Yang V, Hsiao GC, Shuen J-S, Hsieh K-C. Droplet behavior at supercritical conditions, vol. 1, AIAA; 1996. p. 413–437.

[30] Chae JW, Yang HS, Yoon WS. Supercritical droplet dynamics and emission in low speed cross-flows. J Mech Sci Technol 2009;22(8):1586–601. http://dx.doi.org/10.1007/s12206-008-0431-8.

[31] Han J, Tryggvason G. Secondary breakup of axisymmetric liquid drops. I. Acceleration by a constant body force. Phys Fluids 1999;11(12):3650–67. http://dx.doi.org/10.1063/1.870229.

[32] Lemmon E, McLinden M, Friend D. Thermophysical Properties of Fluid Systems, National Institute of Standards and Technology, Gaithersburg MD, 20899. http://webbook.nist.gov.

[33] Guildenbecher DR, López-Rivera C, Sojka PE. Secondary atomization. Exp Fluids 2009;46(3):371–402. http://dx.doi.org/10.1007/s00348-008-0593-2.

[34] Raghuram S, Raghavan V, Pope DN, Gogos G. Two-phase modeling of evaporation characteristics of blended methanol–ethanol droplets. Int J Multiph Flow 2013;52:46–59. http://dx.doi.org/10.1016/j.ijmultiphaseflow.2012.12.008.

[35] Castanet G, Frackowiak B, Tropea C, Lemoine F. Heat convection within evaporating droplets in strong aerodynamic interactions. Int J Heat Mass Transfer 2011;54(15–16):3267–76. http://dx.doi.org/10.1016/j.ijheatmasstransfer.2011.03.060.

[36] Marchese AJ, Dryer FL. The effect of liquid mass transport on the combustion and extinction of bicomponent droplets of methanol and water. Combust Flame 1996;105(1):104–22. http://dx.doi.org/10.1016/0010-2180(95)00179-4.

[37] Saengkaew S, Charinpanitkul T, Vanisri H, Tanthapanichakoon W, Biscos Y, Garcia N, Lavergne G, Mees L, Gouesbet G, Gréhan G. Rainbow refractometry on particles with radial refractive index gradients. Exp Fluids 2007;43 (4):595–601. http://dx.doi.org/10.1007/s00348-007-0342-y.

[38] Wu X, Jiang H, Wu Y, Song J, Gréhan G, Saengkaew S, Chen L, Gao X, Cen K. One-dimensional rainbow thermometry system by using slit apertures. Opt Lett 2014;39(3):638–41. http://dx.doi.org/10.1364/OL.39.000638.